J|A|C|S
ARTICLES
Published on Web 11/10/2005

Kinetically Controlled Synthesis of Triangular and Hexagonal Nanoplates of Palladium and Their SPR/SERS Properties

Yujie Xiong,[†] Joseph M. McLellan,[†] Jingyi Chen,[†] Yadong Yin,[‡] Zhi-Yuan Li,[§] and Younan Xia*,[†]

Contribution from the Department of Chemistry, University of Washington, Seattle, Washington 98195, The Molecular Foundry, Lawrence Berkeley National Laboratory, Berkeley, California 94720, and Institute of Physics, Chinese Academy of Sciences, Beijing 100080, P. R. China

Received September 21, 2005; E-mail: xia@chem.washington.edu

Abstract: The rapid reduction of Na_2PdCl_4 by ethylene glycol in the presence of poly(vinyl pyrrolidone) (PVP) has recently been demonstrated as a convenient method of generating Pd cubooctahedra and twinned nanoparticles. Here we describe a new procedure where Pd triangular or hexagonal nanoplates could be selectively synthesized by manipulating the reduction kinetics of the polyol process. More specifically, the reduction rate was substantially reduced through the introduction of Fe(III) species and the O_2/Cl^- pair, two wet etchants for Pd(0). The etching power of the O_2/Cl^- pair could be further enhanced by adding an acid to lower the pH of the reaction solution. Unlike the previously reported synthesis of Ag and Au nanoplates, light was found to have no indispensable role in the formation of Pd nanoplates. Both triangular and hexagonal nanoplates of Pd exhibited surface plasmon resonance (SPR) peaks in the visible region, and their positions matched with the results of discrete dipole approximation (DDA) calculation. Thanks to their sharp corners and edges, these Pd nanoplates could serve as active substrates for surface-enhanced Raman scattering (SERS).

Introduction

Synthesis of metal nanostructures has been a research theme for decades as driven by their widespread use in catalysis, photography, photonics, electronics, optoelectronics, plasmonics, information storage, optical sensing, biological labeling, imaging, and surface-enhanced Raman scattering (SERS).[1−6] The properties of metal nanostructures are determined by their size, shape, composition, crystallinity, and structure (e.g. solid versus hollow).[3a,7] One can, in principle, control any one of these parameters to tailor their properties for various applications. Recently, shape control has received considerable attention,[8] because in many cases it allows one to fine-tune the properties with a greater versatility than can be achieved otherwise. For instance, as it has been predicted by computational studies and confirmed by experimental work, the number and position of surface plasmon resonance (SPR) peaks, as well as the effective spectral range for SERS, can both be easily tuned by controlling the shape of metal nanostructures.[2e,6d,8e,9,10] To date, shape-controlled synthesis has been achieved for a number of metals and alloys, including Co, Ag, Au, Pt, Pd, Rh, Ir, and FePt. Most

[†] University of Washington.
[‡] Lawrence Berkeley National Laboratory.
[§] Chinese Academy of Sciences.

(1) Reviews: (a) Halperin, W. P. *Rev. Mod. Phys.* **1986**, *58*, 533. (b) Templeton, A. C.; Wuelfing, W. P.; Murray, R. W. *Acc. Chem. Res.* **2000**, *33*, 27.
(2) Catalysis, photography, and photonics: (a) Lam, D. M.-K.; Rossiter, B. W. *Sci. Am.* **1991**, *265*, 80. (b) Lewis, L. N. *Chem. Rev.* **1993**, *93*, 2693. (c) Ahmadi, T. S.; Wang, Z. L.; Green, T. C.; Henglein, A.; El-Sayed, M. A. *Science* **1996**, *272*, 1924. (d) Maier, S. A.; Brongersma, M. L.; Kik, P. G.; Meltzer, S.; Requicha, A. A. G.; Atwater, H. A. *Adv. Mater.* **2001**, *13*, 1501. (e) Murphy, C. J.; Jana, N. R. *Adv. Mater.* **2002**, *14*, 80. (f) Teng, X.; Black, D.; Watkins, N. J.; Gao, Y.; Yang, H. *Nano Lett.* **2003**, *3*, 261.
(3) Electronics and optoelectronics: (a) El-Sayed, M. A. *Acc. Chem. Res.* **2001**, *34*, 257. (b) Chen, S.; Yang, Y. *J. Am. Chem. Soc.* **2002**, *124*, 5280.
(4) Information storage: (a) Peyser, L. A.; Vinson, A. E.; Bartko, A. P.; Dickson, R. M. *Science* **2001**, *291*, 103. (b) Murray, C. B.; Sun, S.; Doyle, H.; Betley, T. *MRS Bull.* **2001**, *26*, 985.
(5) Labeling, imaging, and sensing: (a) Taton, T. A.; Mirkin, C. A.; Letsinger, R. L. *Science* **2000**, *289*, 1757. (b) Nicewarner-Peña, S. R.; Freeman, R. G.; Reiss, B. D.; He, L.; Peña, D. J.; Walton, I. D.; Cromer, R.; Keating, C. D.; Natan, M. J. *Science* **2001**, *294*, 137. (c) Tkachenko, A. G.; Xie, H.; Coleman, D.; Glomm, W.; Ryan, J.; Anderson, M. F.; Franzen, S.; Feldheim, D. L. *J. Am. Chem. Soc.* **2003**, *125*, 4700. (d) Zhang, X.; Young, M. A.; Lyandres, O.; Van Duyne, R. P. *J. Am. Chem. Soc.* **2005**, *127*, 4484. (e) Chen, J.; Saeki, F.; Wiley, B. J.; Cang, H.; Cobb, M. J.; Li, Z.-Y.; Au, L.; Zhang, H.; Kimmey, M. B.; Li, X.; Xia, Y. *Nano Lett.* **2005**, *5*, 473.
(6) SERS: (a) Nie, S.; Emory, S. R. *Science* **1997**, *275*, 1102. (b) Tessier, P. M.; Velev, O. D.; Kalambur, A. T.; Rabolt, J. F.; Lenhoff, A. M.; Kaler, E. W. *J. Am. Chem. Soc.* **2000**, *122*, 9554. (c) Cao, Y. C.; Jin, R.; Mirkin, C. A. *Science* **2002**, *297*, 1536. (d) Dick, L. A.; McFarland, A. D.; Haynes, C. L.; Van Duyne, R. P. *J. Phys. Chem. B* **2002**, *106*, 853. (e) Haes, A. J.; Haynes, C. L.; McFarland, A. D.; Schatz, G. C.; Van Duyne, R. P.; Zhou, S. *MRS Bull.* **2005**, *30*, 368.
(7) (a) Kreibig, U.; Vollmer, M. *Optical Properties of Metal Clusters*; Springer: New York, 1995. (b) Jackson, J. B.; Halas, N. J. *J. Phys. Chem. B* **2001**, *105*, 2473.
(8) (a) Sun, S.; Murray, C. B.; Weller, D.; Folks, L.; Moser, A. *Science* **2000**, *287*, 1989. (b) Chen, S.; Wang, Z. L.; Ballato, J.; Foulger, S. H.; Carroll, D. L. *J. Am. Chem. Soc.* **2003**, *125*, 16186. (c) Caswell, K. K.; Wilson, J. N.; Bunz, U. H. F.; Murphy, C. J. *J. Am. Chem. Soc.* **2003**, *125*, 13914. (d) Kim, F.; Connor, S.; Song, H.; Kuykendall, T.; Yang, P. *Angew. Chem., Int. Ed.* **2004**, *43*, 3673. (e) Narayanan, R.; El-Sayed, M. A. *J. Phys. Chem. B* **2004**, *108*, 5726. (f) Hao, E.; Bailey, R. C.; Schatz, G. C.; Hupp, J. T.; Li, S. *Nano Lett.* **2004**, *4*, 327. (g) Yin, Y.; Rioux, R. M.; Erdonmez, C. K.; Hughes, S.; Somorjai, G. A.; Alivisatos, A. P. *Science* **2004**, *304*, 711.
(9) (a) Jensen, T. R.; Kelly, L.; Lazarides, A.; Schatz, G. C. *J. Cluster Sci.* **1999**, *10*, 295. (b) Kottmann, J. P.; Martin, O. J. F.; Smith, D. R.; Schultz, S. *Phys. Rev. B* **2001**, *64*, 235402. (c) Sosa, I. O.; Noguez, C.; Barrera, R. G. *J. Phys. Chem. B* **2003**, *107*, 6269.
(10) (a) Muniz-Miranda, M. *Chem. Phys. Lett.* **2001**, *340*, 437. (b) Im, S. H.; Lee, Y. T.; Wiley, B.; Xia, Y. *Angew. Chem., Int. Ed.* **2005**, *44*, 2154.

10.1021/ja056498s CCC: $30.25

of these procedures involve the reduction of salt compounds or thermal decomposition of organometallic precursors in the presence of surfactants, polymers, biomolecules, and coordinating ligands and sometimes with the mediation of seeds.[8]

As a noble metal, Pd plays a central role in many industrial applications.[11,12] For example, it serves as the primary catalyst for low-temperature reduction of automobile pollutants[11] and for organic reactions such as Suzuki, Heck, and Stille coupling.[12] To maximize the performance in these applications, a great deal of efforts has been devoted to the synthesis of Pd nanostructures: Pd nanoparticles of various morphologies have been prepared in the presence of surfactants or polymers, with the mediation of RNAs, through the decomposition of a Pd−surfactant complex, or via the direction of a coordinating ligand.[13] The control knobs of all these syntheses have been largely limited to temperature, the concentration of precursor, and the surfactant or polymer. The ability to control and fine-tune the shape of Pd nanostructures has been modestly successful. It still remains a grand challenge to deterministically generate a specific shape.

Another important property of Pd nanoparticles that remains largely unexplored is their SPR features, which could lead to applications in colorimetric sensing, plasmonic waveguiding, enhancement of electromagnetic fields and light transmission, and optical sensing of hydrogen.[14] The SPR peak of small Pd nanoparticles (typically <10 nm in size) is located in the UV region, which gives them an uninteresting black color and makes their SPR characteristics much more difficult to probe due to the strong absorption of light at these wavelengths by glass and most solvents.[15] Recently we found that the SPR peak of Pd nanocubes could be shifted to the visible region by increasing their sizes to >25 nm.[16a] Using the discrete dipole approximation (DDA) method,[9c,17] it was also found that the SPR features could be further tailored through shape control. The position of the SPR peak determines not only the color of a colloidal suspension but also the wavelength of excitation, at which one would obtain the maximum electromagnetic field enhancement. A strong local electric field is crucial to the enhancement of Raman and other spectroscopic signals.[17a] It has been reported that metal nanostructures with sharp corners or edges are especially active SERS substrates, and the local value of $|E|^2$ could be more than 500 times that of the applied field.[17b] All these challenges and opportunities have inspired us to systematically investigate shape-controlled synthesis of Pd nanostructures.

This paper describes the facile synthesis of Pd triangular and hexagonal nanoplates using a modified polyol process. Polyol reduction has long been known as a simple and versatile method for producing metal nanoparticles.[18] We have recently redesigned this method for generating metal nanostructures with well-controlled shapes.[19] Here we demonstrate that oxidative etching by Fe(III) species and the Cl^-/O_2 pair, when coupled with polyol reduction, could significantly alter the reduction kinetics of Pd precursor and, thus, induce the formation of triangular and hexagonal nanoplates. We have also investigated their SPR properties and examined their potential as SERS substrates. Our results clearly demonstrate that Pd will provide another interesting and useful system for both plasmonic and SERS applications.

Experimental Section

Chemicals and Materials. Ethylene glycol (EG, J. T. Baker, 9300-01), sodium palladium(II) chloride (Na_2PdCl_4, Aldrich, 379808-1g), poly(vinyl pyrrolidone) (PVP, Aldrich, 856568-100g, MW = 55 000), and anhydrous ferric chloride ($FeCl_3$, Fisher, I89-100g) were all used as received without further purification.

Synthesis of Pd Triangular Nanoplates. In a typical synthesis, 5 mL of EG was placed in a three-neck flask (equipped with a reflux condenser and a Teflon-coated magnetic stirring bar) and heated in air at 85 °C for 1 h. Meanwhile, 0.0162 g of Na_2PdCl_4 and 0.0312 g of PVP were separately dissolved in 3 mL of EG at room temperature, followed by the addition of 55 μL of aqueous HCl solution (1.0 M) to the Pd precursor solution. After 20 μL of 0.2 M $FeCl_3$ solution in EG was added to the flask, the two solutions of Pd precursor and PVP (with the molar ratio between Pd and the repeating unit of PVP being 1:5) were simultaneously injected through a two-channel syringe pump (KDS-200, Stoelting, Wood Dale, IL) at a rate of 12 mL/h. The reaction mixture was continued with heating at 85 °C in air for 4.5 h. The product was centrifuged and washed with acetone once and then with ethanol three times to remove EG and excess PVP. The as-obtained sample was characterized using transmission electron microscopy (TEM), electron diffraction (ED), high-resolution TEM (HRTEM), powder X-ray diffraction (PXRD), and UV−vis spectroscopy.

Synthesis of Pd Hexgonal Nanoplates. The procedure was similar to what was used for the triangular nanoplates, except that 40 μL (instead of 20 μL) of 0.2 M $FeCl_3$ solution was added to the reaction system before introducing the Pd precursor and PVP.

SERS Measurements. The samples for SERS studies were prepared by drying 3 μL of the aqueous sols on an Al film (25 nm) thermally evaporated onto a Si wafer. The substrate was incubated in a 4 mM aqueous 4-mercaptopyridine solution for 1 h, rinsed with deionized water, and dried with a stream of air. SERS spectra were obtained at a laser excitation wavelength of 785 nm using a Leica DM IRBE optical microscope equipped with a Renishaw inVia Raman system (HPNIR785) and a thermoelectrically cooled CCD detector. The spot size was 1.6 μm, and the laser power was 3 mW at the sample surface.

Instrumentation. All TEM images were taken using a Phillips 420 transmission electron microscope operated at 120 kV. HRTEM images and ED patterns were taken on a JEOL 2010 LaB6 high-resolution transmission electron microscope operated at 200 kV. The samples for TEM studies were prepared by drying a drop of the aqueous suspension of particles on a piece of carbon-coated copper grid (Ted Pella, Redding, CA) under ambient conditions. The grid was then transferred to a

(11) See, for example: (a) Fernández-García, M.; Martínez-Arias, A.; Salamanca, L. N.; Coronado, J. M.; Anderson, J. A.; Conesa, J. C.; Soria, J. *J. Catal.* **1999**, *187*, 474. (b) Nishihata, Y.; Mizuki, J.; Akao, T.; Tanaka, H.; Uenishi, M.; Kimura, M.; Okamoto, T.; Hamada, N. *Nature* **2002**, *418*, 164.
(12) See, for example: (a) Reetz, M. T.; Westermann, E. *Angew. Chem., Int. Ed.* **2000**, *39*, 165. (b) Franzén, R. *Can. J. Chem.* **2000**, *78*, 957. (c) Li, Y.; Hong, X. M.; Collard, D. M.; El-Sayed, M. A. *Org. Lett.* **2000**, *2*, 2385. (d) Kim, S.-W.; Kim, M.; Lee, W. Y.; Hyeon, T. *J. Am. Chem. Soc.* **2002**, *124*, 7642. (e) Son, S. U.; Jang, Y.; Park, J.; Na, H. B.; Park, H. M.; Yun, H. J.; Lee, J.; Hyeon, T. *J. Am. Chem.* Soc. **2004**, *126*, 5026.
(13) (a) Teranishi, T.; Miyake, M. *Chem. Mater.* **1998**, *10*, 594. (b) Bradley, J. S.; Tesche, B.; Busser, W.; Maase, M.; Reetz, M. T. *J. Am. Chem. Soc.* **2000**, *122*, 4631. (c) Kim, S.-W.; Park, J.; Jang, Y.; Chung, Y.; Hwang, S.; Hyeon, T.; Kim, Y. W. *Nano Lett.* **2003**, *3*, 1289. (d) Veisz, B.; Király, Z. *Langmuir* **2003**, *19*, 4817. (e) Son, S. U.; Jang, Y.; Yoon, K. Y.; Kang, E.; Hyeon, T. *Nano Lett.* **2004**, *4*, 1147. (f) Gugliotti, L. A.; Feldheim, D. L.; Eaton, B. E. *Science* **2004**, *304*, 850.
(14) (a) Tobiška, P.; Hugon, O.; Trouillet, A.; Gagnaire, H. *Sens. Actuators* **2001**, *74*, 168. (b) Xia, Y.; Halas, N. J. *MRS Bull.* **2005**, *30*, 338.
(15) Creighton, J. A.; Eadon, D. G. *J. Chem. Soc., Faraday Trans.* **1991**, *87*, 3881.
(16) (a) Xiong, Y.; Chen, J.; Wiley, B.; Xia, Y.; Yin, Y.; Li, Z.-Y. *Nano Lett.* **2005**, *5*, 1237. (b) Xiong, Y.; Wiley, B.; Chen, J.; Li, Z.-Y.; Yin, Y.; Xia, Y. *Angew. Chem., Int. Ed.* **2005**, in press.
(17) (a) Yang, W. H.; Schatz, G. C.; Van Duyne, R. P. *J. Chem. Phys.* **1995**, *103*, 869. (b) Kelly, K. L.; Coronado, E.; Zhao, L. L.; Schatz, G. C. *J. Phys. Chem. B* **2003**, *107*, 668.
(18) Fievet, F.; Lagier, J. P.; Figlarz, M. *MRS Bull.* **1989**, *14*, 29.
(19) (a) Sun, Y.; Xia, Y. *Science* **2002**, *298*, 2176. (b) Chen, J.; Herricks, T.; Geissler, M.; Xia, Y. *J. Am. Chem. Soc.* **2004**, *126*, 10854. (c) Wiley, B.; Herricks, T.; Sun, Y.; Xia, Y. *Nano Lett.* **2004**, *4*, 1733. (d) Wiley, B.; Sun, Y.; Mayers, B.; Xia, Y. *Chem.*—Eur. J. **2005**, *11*, 455.

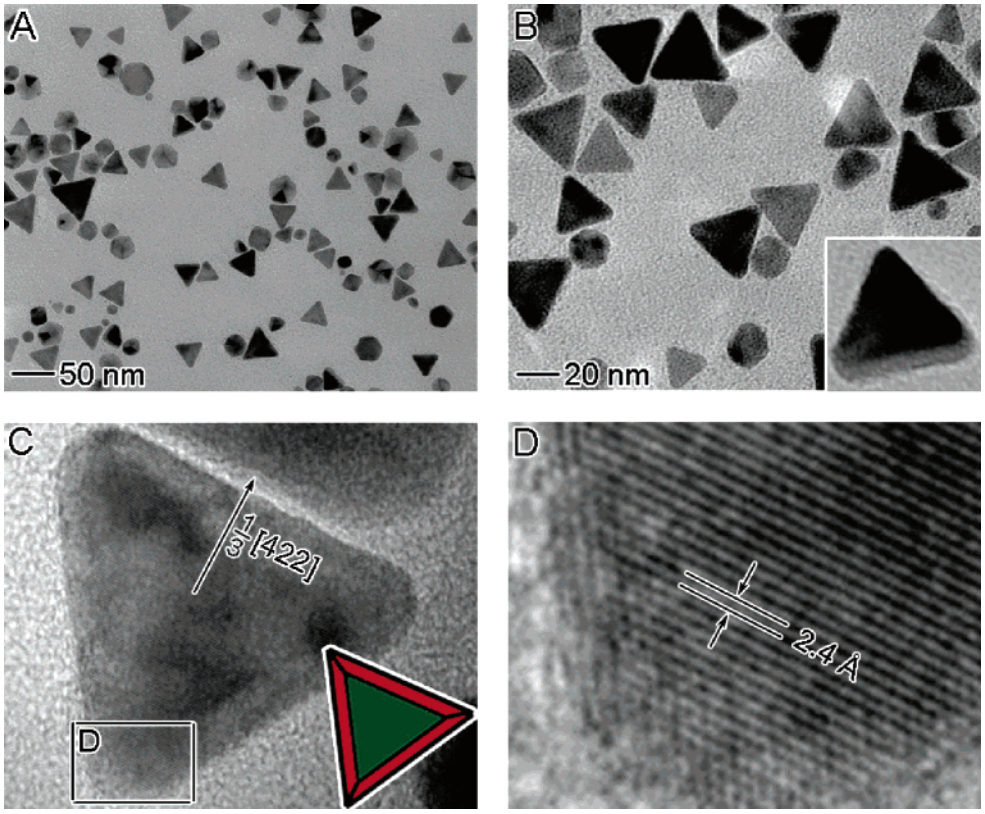

Figure 1. Electron microscopy characterization of Pd triangular nanoplates prepared at 85 °C in the presence of 0.36 mM $FeCl_3$ and 5 mM HCl, with the molar ratio of PVP to Pd precursor being 5 (concentrations given in all figure captions are the final values in the reaction solution): (A, B) TEM images; (C, D) high-resolution TEM images. The inset in (B) gives the TEM image of a titled triangular nanoplate showing one of its side faces. The inset of (C) shows a schematic drawing of the triangular nanoplate, where the red and green colors represent the {100} and {111} facets, respectively.

gravity-fed flow cell and washed for 1 h with deionized water to remove the excess PVP. Finally, the sample was dried and stored in a vacuum for TEM characterization. Powder XRD patterns were recorded on a Philips 1820 diffractometer equipped with a Cu Kα radiation source (λ = 1.541 80 Å). UV−vis extinction spectra were taken using a Hewlett-Packard 8452A diode array spectrophotometer.

Results and Discussion

The essence of polyol synthesis is the reduction of a metal salt by EG in the presence of PVP. Palladium atoms can be produced by reducing a precursor such as $PdCl_4^{2-}$ with EG through the following two steps:[18]

$$2HOCH_2CH_2OH \rightarrow 2CH_3CHO + 2H_2O \quad (1)$$

$$PdCl_4^{2-} + 2CH_3CHO \rightarrow CH_3CO{-}OCCH_3 + Pd + 2H^+ + 4Cl^- \quad (2)$$

Like other face-centered cubic (fcc) noble metals, the thermodynamically favorable shapes of Pd nanocrystals are cubooctahedra and multiple twinned particles (MTPs). When $PdCl_4^{2-}$ is reduced by EG to generate Pd(0) atoms at a sufficiently high rate, the final product will have no choice but to take the thermodynamically favored shapes. When the reduction becomes substantially slow, however, the nucleation and growth will be turned into kinetic control and the final product can take a range of shapes deviated from the thermodynamic ones.

In our previous studies, it was found that when $PdCl_4^{2-}$ was added to EG heated to an elevated temperature, the rapid reduction (within ~5 min) of $PdCl_4^{2-}$ by EG produced 90% Pd cubooctahedra and 10% MTPs of 8−10 nm in size.[20] These results confirm that cubooctahedra and MTPs of Pd have relatively low surface free energies and are thereby favored by thermodynamics. Therefore, for the synthesis of Pd nanoplates, one must carefully control the reduction kinetics, particularly at the seeding stage, as formation of these highly anisotropic structures only become favorable in a slow reduction process.[21] Several research groups have employed such a kinetic control to obtain triangular and circular nanoplates of Ag in a number of different solvents.[22] The success of the present synthesis is based on the oxidative etching of Pd(0) by $FeCl_3$ and the Cl^-/O_2 pair; both of them can be added with good precision to tightly control the reduction kinetics of $PdCl_4^{2-}$ and thus obtain highly anisotropic nanostructures.

Structural Analysis of the Pd Triangular Nanoplates. Figure 1A,B shows the TEM images of a typical product which contained 70% triangular nanoplates of ~28 nm in edge length and 30% cubooctahedral and twinned nanoparticles of 8−20 nm in size. The inset of Figure 1B shows the TEM image of a titled nanoplate, from which the thickness of the plate was estimated to be around 5 nm. Figure 1C,D shows the HRTEM

(20) Xiong, Y.; Chen, J.; Wiley, B.; Xia, Y.; Aloni, S.; Yin, Y. *J. Am. Chem. Soc.* **2005**, *127*, 7332.
(21) Mullin, J. W. *Crystallization*; Butterworth: London, 1961.
(22) (a) Jin, R.; Cao, Y.; Mirkin, C. A.; Kelly, K. L.; Schatz, G. C.; Zheng, J. G. *Science* **2001**, *294*, 1901. (b) Chen, S.; Carroll, D. L. *Nano Lett.* **2002**, *2*, 1003. (c) Chen, S.; Fan, Z.; Carroll, D. L. *J. Phys. Chem. B* **2002**, *106*, 10777. (d) Pastoriza-Santos, I.; Liz-Marzán, L. M. *Nano Lett.* **2002**, *2*, 903. (e) Yener, D. O.; Sindel, J.; Randall, C. A.; Adair, J. H. *Langmuir* **2002**, *18*, 8692. (f) Maillard, M.; Giorgio, S.; Pileni, M.-P. *Adv. Mater.* **2002**, *14*, 1084. (g) Jin, R.; Cao, Y. C.; Hao, E.; Metraux, G. S.; Schatz, G. C.; Mirkin, C. A. *Nature* **2003**, *425*, 487.

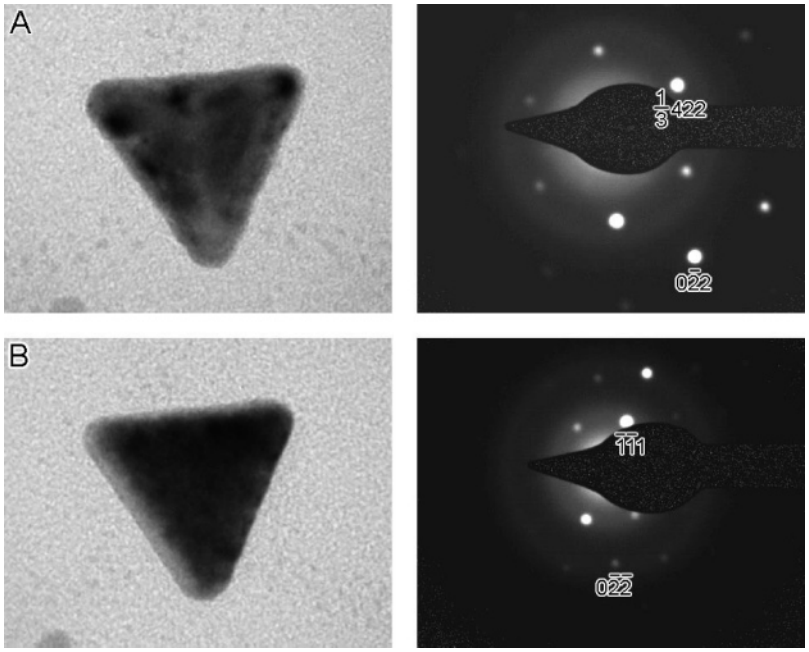

Figure 2. (A) ED pattern taken from an individual Pd triangular nanoplate (shown by the TEM image in the left panel) by directing the electron beam perpendicular to its triangular faces. (B) ED pattern taken from the edge of this nanoplate (shown by the TEM image in the left panel) by tilting the nanoplate by 35°.

images of a nanoplate recorded along the [$\bar{1}$11] zone axis. The fringes in Figure 1D are separated by 2.4 Å, which can be ascribed to the 1/3{422} reflection that is usually forbidden for an fcc lattice.

Figure 2A shows the ED pattern recorded by directing the electron beam perpendicular to the triangular flat faces of an individual nanoplate. The 6-fold rotational symmetry of the diffraction spots implies that the triangular faces are actually presented by {111} planes. Two sets of spots can be identified based on their *d* spacing: the outer set with a spacing of 1.4 Å is due to the {220} reflection of fcc Pd, and the inner set with a lattice spacing of 2.4 Å is believed to originate from the forbidden 1/3{422} reflection. The forbidden 1/3{422} reflection has also been observed in Ag or Au nanostructures in the form of thin plates or films bounded by atomically flat surfaces.[22,24] It should be pointed out that the 1.4 Å *d* spacing of the {220} planes is beyond the resolution of our microscope, and hence the {220} fringes were not observed in the HRTEM images. Figure 2B shows a diffraction pattern of the side face recorded in the [011] orientation when the nanoplate was titled by 35°. This pattern confirms that the side faces of each nanoplate are bound by the {100} planes. With these observations combined, it can be concluded that the Pd triangular nanoplates are bound by two {111} planes as the top and bottom faces and three {100} planes as the side faces. A schematic illustration is shown in the inset of Figure 1C. These assignments are similar to the results previously reported for triangular nanoplates of Ag and Au.[22,23]

The phase purity and high crystallinity of the Pd triangular nanoplates is also supported by powder X-ray diffraction. Figure S1 shows the typical PXRD pattern of an as-prepared sample; all the peaks can be assigned to fcc Pd (JCPDS card, 05-0681). It is worth noting that the ratio between the intensities of (111) and (200) peaks is much higher than the index value (2.89 versus 2.38), indicating that the top and bottom faces of each nanoplate are bounded by {111} planes. These nanoplates are more or less oriented parallel to the supporting substrate, resulting in a stronger (111) diffraction peak than that of a conventional powder sample.

Roles of Fe(III) and Oxygen. Although the reduction kinetics can often be controlled by varying experimental parameters such as temperature, here we found that the introduction of an etchant such as Fe(III) species or the O_2/Cl^- pair was more convenient and versatile. For instance, we have performed the synthesis at 70, 50, and 30 °C without adding $FeCl_3$ and HCl. While the reduction became notably slower at both 70 and 50 °C, it was still too fast to generate Pd nanoplates. Cuboctahedra were obtained as the major species in these two products. At 30 °C, the reduction of Pd precursor ceased and no Pd nanoparticles were observed even after several days. These observations can be understood in terms of the Arrhenius equation

$$\ln k = (-E_a/RT) + B \qquad (3)$$

where *k* is the rate constant and E_a is the activation energy. For this exponential process, control of reduction kinetic via change of temperature alone becomes extremely difficult due to the nonlinearity and high sensitive toward temperature.

Different from temperature control, oxidative etching provides a simple and versatile means of manipulating the reduction kinetics. As we have demonstrated in previous studies, the O_2/Cl^- pair was able to selectively remove twinned particles involved in the polyol synthesis of Ag and Pd nanostructures, leaving behind only single-crystal cuboctahedra in the final products.[19,20] In the present case, however, etching by O_2/Cl^- alone could not sufficiently slow the reduction to achieve anisotropic growth and form thin nanoplates. This is mainly

(23) Wang, Z. L. *J. Phys. Chem. B* **2000**, *104*, 1153.
(24) (a) Kirkland, A. I.; Jefferson, D. A.; Duff, D. G.; Edwards, P. P.; Gameson, I.; Johnson, B. F. G.; Smith, D. J. *Proc. R. Soc. London, Ser. A* **1993**, *440*, 589. (b) Germain, V.; Li, J.; Ingert, D.; Wang, Z. L.; Pileni, M. P. *J. Phys. Chem. B* **2003**, *107*, 8717. (c) Sun, Y.; Xia, Y. *Adv. Mater.* **2003**, *15*, 695. (d) Sun, Y.; Mayers, B.; Xia, Y. *Nano Lett.* **2003**, *3*, 675.

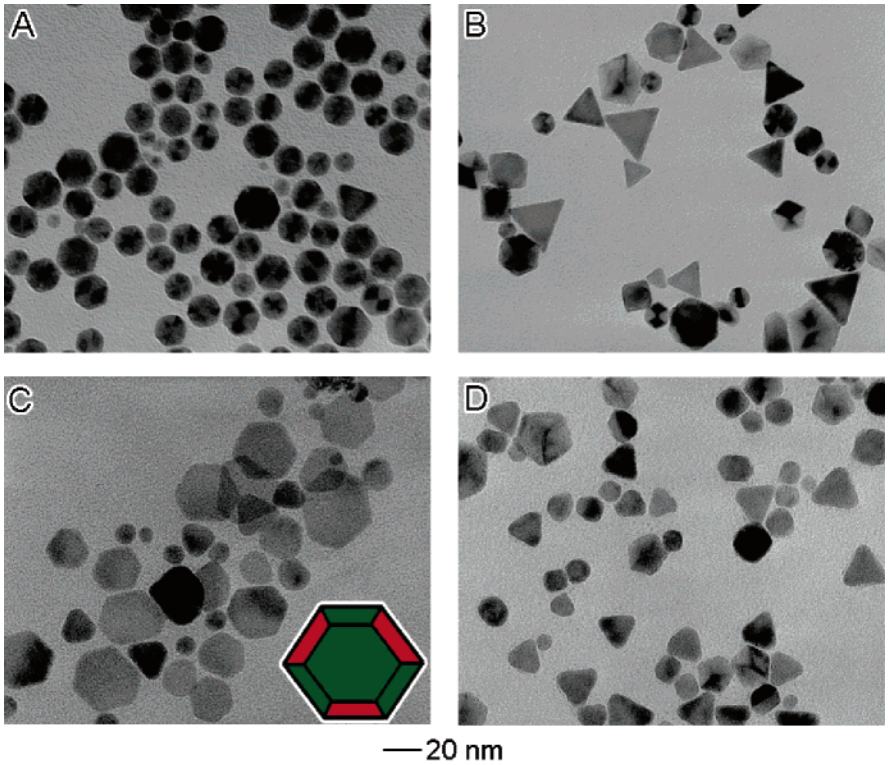

Figure 3. TEM images of four as-obtained samples illustrating the variation in morphology by changing the amount of $FeCl_3$ or excluding air from the system, while other parameters were kept the same as in Figure 1 (at 85 °C, in the presence of 5 mM HCl, and with the molar ratio of PVP to Pd precursor being 5): (A) no $FeCl_3$; (B) 0.18 mM $FeCl_3$; (C) 0.72 mM $FeCl_3$; (D) 0.36 mM $FeCl_3$. The syntheses of (A)−(C) were performed in air while the synthesis of (D) was conducted under continuous bubbling of Ar. The inset in (C) shows a schematic drawing of the hexagonal nanoplate, where the red and green colors represent the {100} and {111} facets, respectively.

limited by the low level of O_2 dissolved in EG and/or adsorbed on the surface of Pd particles. To solve this problem, we explored other oxidative etchants that could be quantitatively added to the reaction solution. Ferric species is a well-established, effective wet etchant for noble metals.[25] As suggested by the standard potentials of the redox pairs involved in this system, Fe(III) could oxidize Pd(0) back to Pd(II), competing with reaction 2, and thus reducing the overall formation rate of Pd(0):[26]

$$Fe^{3+} + e^- \rightarrow Fe^{2+} \quad E^\circ = 0.77\ V \tag{4}$$

$$PdCl_4^{2-} + 2e^- \rightarrow Pd + 4Cl^- \quad E^\circ = 0.59\ V \tag{5}$$

Most recently, we also discovered that the introduction of Fe(III) species into the synthesis of Pd nanocubes could reduce the nucleation density and thus produce relatively large nanocubes.[16a] As indicated by the change of color from yellow-brown to dark brown, the reduction was retarded for almost 8 min when 1.25 mM $FeCl_3$ was used. In the present synthesis, the etching powers of both Fe(III) species and the O_2/Cl^- pair were added together to achieve a tighter control over the reduction kinetics. Furthermore, simultaneous introduction of an acid such as HCl also enhanced the etching powder of the O_2/Cl^- pair. Combined together, the polyol reduction time of $PdCl_4^{2-}$ could be stretched from less than 5 min to 1 h to significantly decrease the supersaturation of Pd atoms and alter the growth kinetics of Pd nanoparticles.

On the basis of the above arguments, the concentration of Fe(III) species should play a critical role in controlling the reduction kinetics and thus the morphology of resultant Pd nanostructures. We have confirmed that both the retardation of reduction and the morphology of final product were strongly dependent on the concentration of $FeCl_3$. As shown in Figure 3A, the sample mainly consisted of cubooctahedral nanoparticles in the absence of $FeCl_3$. As the concentration of $FeCl_3$ was increased to 0.18 and 0.36 mM, the product contained 35% (Figure 3B) and 70% (Figure 1B) triangular nanoplates, respectively. However, if the concentration of $FeCl_3$ exceeded 0.36 mM, the major product became hexagonal plates, which represent another kinetically controlled morphology. Figure 3C shows the TEM image of a sample prepared with the addition of 0.72 mM $FeCl_3$. These results clearly demonstrated that addition of Fe(III) species can lead to new shapes significantly deviated from the thermodynamically favored ones such as cuboctahedral and twinned nanoparticles.

As discussed by Wang in a review article,[23] the flat top and bottom faces of these hexagonal plates should be bound by {111} planes, and the six side faces by {111} and {100} planes, as shown by the geometrical model in the inset of Figure 3C. These assignments are confirmed by the ED pattern (Figure 4A) taken from an individual nanoplate by directing the electron beam perpendicular to its hexagonal flat faces. Similar to the case of triangular nanoplate, the 6-fold symmetry of the diffraction spots indicates that the hexagonal faces are bound by {111} planes. We can identify two sets of spots, with the outer set being indexed to the {220} reflection of fcc Pd and the inner set to the forbidden 1/3{422} reflection. Figure 4B

(25) Xia, Y.; Kim, E.; Whitesides, G. M. *J. Electrochem. Soc.* **1996**, *143*, 1070.
(26) *Handbook of Chemistry and Physics*, 60th ed.; Weast, R. C., Ed.; CRC Press: Boca Raton, FL, 1980.

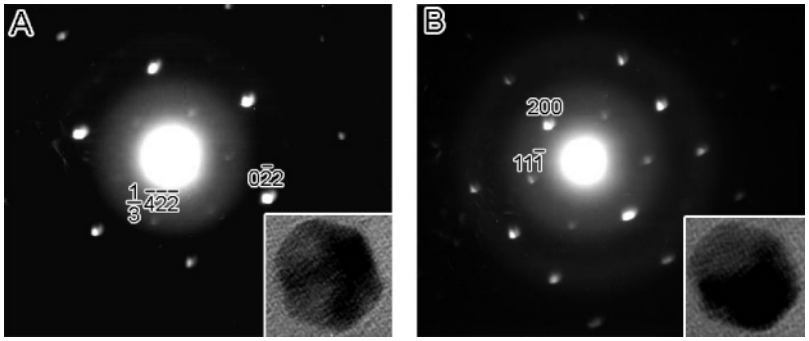

Figure 4. (A) ED pattern taken from an individual Pd hexagonal nanoplate (shown by the TEM image in the inset) by directing the electron beam perpendicular to its hexagonal flat faces. (B) ED pattern taken from the hexagonal faces of the same nanoplate (shown by the TEM image in inset) after it had been titled by 35°.

shows the ED pattern taken along the [011] zone axis when the nanoplate was titled by 35°. On the basis of this diffraction pattern and symmetry consideration, one can deduce that the side faces of a hexagonal nanoplate must be bound by a mix of {100} and {111} planes.

The presence of oxygen from air was also critical to the control of reduction kinetics and hence morphology because it was responsible for the oxidation of Fe(II) back to Fe(III). Without oxygen, the concentration of Fe(III) species in the solution would quickly decrease due to their depletion in the etching process, as well as due to the reduction by EG. As Fe(II) species cannot oxidize Pd(0), the rate at which Pd(0) was etched would be reduced. It should be emphasized that Pd(0) was not etched by Fe(III) alone, the presence of O_2/Cl^- pairs also contributed to the etching process, especially with the addition of an acid. In the absence of air, the reduction rate became notably faster. For these reasons, the percentage of triangular nanoplates in the sample prepared in the absence of air dropped from 70% to 30% (Figure 3D).

It is worth noting that the rates of both reduction and nucleation were extremely slow thanks to the oxidative etching. After the nucleation step, the Pd seeds grew larger as more Pd(0) atoms were added to the surface of seeds. Meanwhile, due to the small number of seeds and the high concentration of Pd precursor in the solution, additional nucleation events might also occur with continuous formation of Pd(0) atoms. In addition, although we could improve the yield of triangular plates by controlling the reduction kinetics, the thermodynamically favored cuboctahedra could not be completely prevented. Taken together, the final product exhibited a relatively broad distribution in size and shape. Further optimization of the experimental condition is needed to improve the uniformity of the sample.

Effect of Acid. As previously stated, an acid could be introduced to enhance the etching power of the O_2/Cl^- pair. This is supported by the standard electrical potentials:[26]

$$O_2 + 4H^+ + 4e^- \rightarrow 2H_2O \quad E^\circ = 1.229\ \text{V} \qquad (6)$$

$$O_2 + 2H_2O + 4e^- \rightarrow 4OH^- \quad E^\circ = 0.401\ \text{V} \qquad (7)$$

According to the Nernst equation, the potential of half reaction 6 is strongly dependent on the concentration of acid. It is clear that the oxidation power of O_2 could be greatly improved by decreasing the pH value of the solution. Hence, the amount of acid added to the reaction solution should be another key parameter in controlling the formation of triangular nanoplates. When the amount of acid was doubled, the reaction would not proceed at 85 °C whether in the presence of Fe(III) species or not, due to extensive etching by O_2/Cl^-. At higher temperature such as 95 °C, the reaction could still be initiated under these conditions, but nanoplates were obtained at low yields (see Figure 5A,B). These results imply that the over etching could be disadvantageous to the formation of uniform nanoplates, even though the reduction rate was substantially reduced. Conversely, if too little acid was added, the reaction would be too fast for nanoplates to form. As an example, Figure 5C shows the result of a typical sample that was prepared when half of the amount of acid for Figure 1 was used. This sample mainly consists of cuboctahedral and twinned nanoparticles. Interestingly, in this case, the reduction kinetics could be regulated by controlling the concentration of Fe(III) species and hence improve the yield of nanoplates (see Figure 5D). These studies clearly demonstrate that both the O_2/Cl^- pair and Fe(III) species play important roles as oxidative etchants in the polyol synthesis, illustrating the power and versatility of their combined effects.

Influence of Temperature and Preheating Time. Although temperature control does not provide a useful means to alter the reduction kinetics, selection of an appropriate temperature seems to be instrumental to the achievement of a desirable reduction rate. For example, we have carried out reactions at various temperatures and found that the lowest temperature allowed for polyol reduction was 78 °C. For reactions carried out at temperatures above 78 °C, the reaction rate increased sharply with temperature, as indicated by a quick change in color for the solution (from yellow-brown to dark brown). Figure 6A−C shows TEM images of samples obtained at three different temperatures. We found that both the shape and size of the product depended on temperature in three different ways. First, slow reduction at low temperatures greatly reduced the level of supersaturation and hence the number of seeds formed in the nucleation step. At the same concentration of Pd precursor, a decrease in the number of seeds resulted in the formation of Pd nanoparticles with larger sizes. In comparison with the products shown in Figures 1 and 3, the nanoparticles prepared at 78 °C were much bigger. Second, the reduction rate, depending on the temperature, was critical to the control of reduction kinetics and hence the formation of triangular nanoplates. As temperature was increased, the yield of nanoplates decreased distinctly. Third, oxidative etching of twinned particles could be partially eliminated at low temperatures. As we have demonstrated, the Pd twinned particles in a sample could be selectively removed

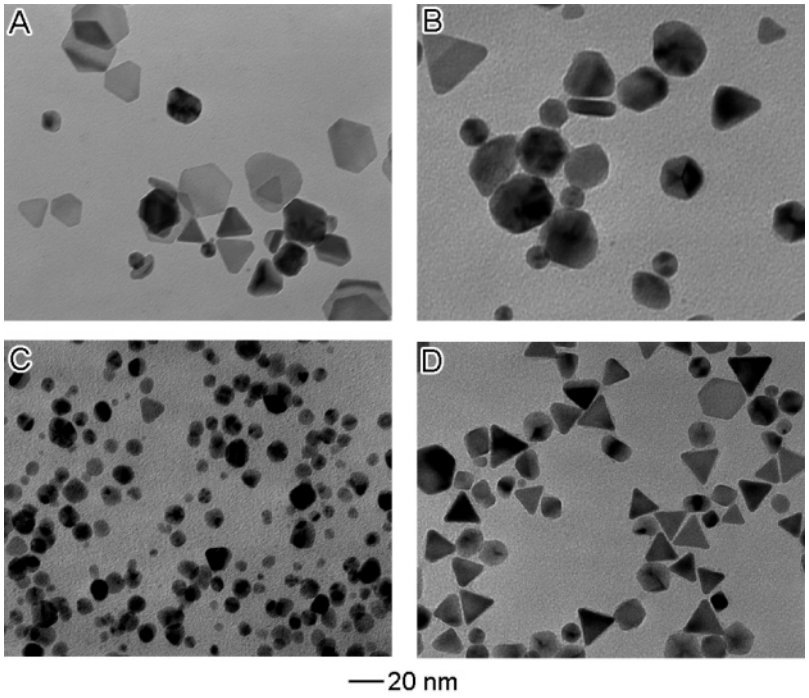

Figure 5. TEM images of four as-obtained samples illustrating the variation in morphology when different experimental conditions were involved (with the molar ratio of PVP to Pd precursor being kept at 5): (A) 10 mM HCl and 0.36 mM $FeCl_3$ at 95 °C; (B) 10 mM HCl and no $FeCl_3$ at 95 °C; (C) 2.5 mM HCl and 0.36 mM $FeCl_3$ at 85 °C; (D) 2.5 mM HCl and 0.72 mM at 85 °C.

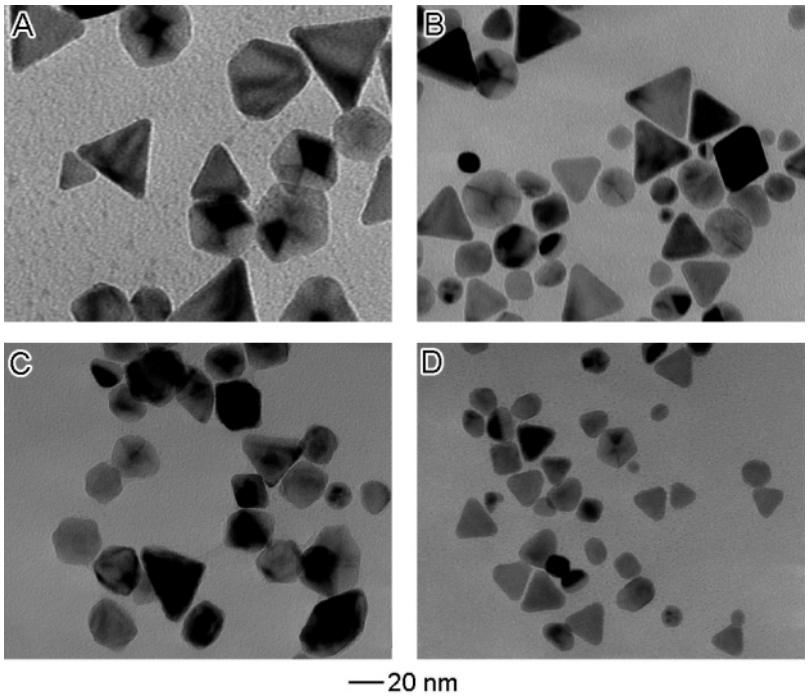

Figure 6. Influence of reaction temperature and preheating time on the morphology of resultant Pd nanostructures. The TEM images were taken from samples prepared at (A) 78 °C, (B) 80 °C, (C) 90 °C, and (D) 85 °C. The ethylene glycol in (A)−(C) was preheated for 1 h while it was preheated for 3 h in synthesis D. All other experimental conditions were the same as those used for the synthesis in Figure 1 (in the presence of 0.36 mM $FeCl_3$ and 5 mM HCl, with the molar ratio of PVP to Pd precursor being 5).

by the O_2/Cl^- pair to leave behind single-crystal cuboctahedra at temperature above 110 °C.[20] In the present system, removal of twinned particles seems to be negligible, especially at relatively low temperatures. As a result, there are more twinned nanoparticles in the sample prepared at a low temperature of 78 °C (see Figure 6A). In general, the product morphology is strongly dependent on temperature, largely due to the influence of temperature on both reduction kinetic and oxidative etching of multiple twinned species.

As described in the Experimental Section, it was necessary to preheat the ethylene glycol for 1 h before injecting Pd precursor and PVP to generate enough aldehyde. As shown in reaction 1, aldehyde is the major reductant involved in a polyol synthesis. It is worth noting that the preheating time is not a

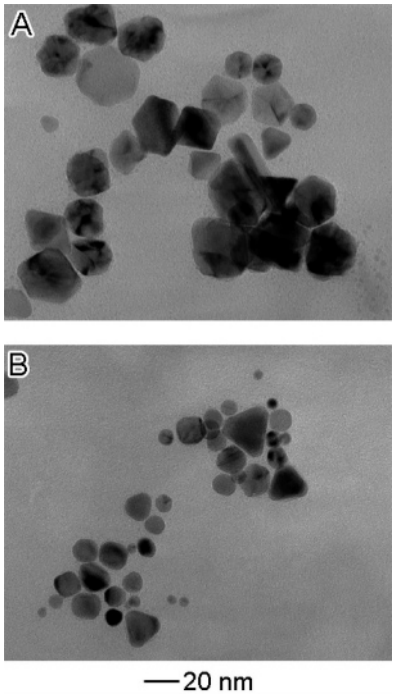

Figure 7. TEM images of two as-synthesized samples illustrating the variation in morphology when different molar ratios between PVP and Pd precursor were used: (A) 1; (B) 25. All other experimental conditions were the same as those used for the synthesis in Figure 1 (at 85 °C in the presence of 0.36 mM $FeCl_3$ and 5 mM HCl).

negligible parameter. If the preheating time was prolonged to 3 h, the reaction generated superfluous aldehyde that would substantially speed up the reduction, resulting in a low yield of triangular nanoplates and a smaller size (see Figure 6D).

Influence of Molar Ratio between PVP and Pd Precursor. The exact role of PVP in controlling the formation of Pd triangular nanoplates is yet to be completely understood. We believe that the major function of PVP was to prevent the Pd nanoparticles from growing too large or aggregating into large entities in the nucleation stage.

The percentage of Pd triangular nanoplates in the final product, as well as the morphology of other Pd structures produced during the reaction, was found to strongly depend on the molar ratio between PVP and Pd precursor. When this ratio was around 5, the content of Pd triangular nanoplates contained in the as-synthesized sample could approach 70%, as shown in Figure 1A. However, if the ratio was decreased or increased to other numbers, the yield of Pd nanoplates in the final product would drop. Figure 7 shows the TEM images of two other samples that were prepared under a condition similar to the one used for Figure 1A, except that the molar ratio of PVP to Pd precursor was varied to values other than 5. Figure 7A shows a typical image of the product where the ratio was reduced to 1. This image implies that the percentage of nanoplates sharply dropped. This result suggests that, with less PVP, the surface of nanoparticles was easily etched so that their morphology was affected. When this ratio was increased to 25, the final product was found to exist as small triangular nanoplates and twinned nanoparticles. As established in a recent study related to the growth of Ag nanowires,[27] the PVP macromolecules were found to interact more strongly with {100} planes than with {111} ones. In the present case, a large quantity of PVP would probably passivate the {100} side faces of nanoplates, resulting in small lateral dimensions. In addition, in the presence of a large quantity of PVP, the twinned particles could be protected from etching by the Cl^-/O_2 pair and therefore be left behind in the final product.

(27) Sun, Y.; Mayers, B.; Herricks, T.; Xia, Y. *Nano Lett.* **2003**, *3*, 955.

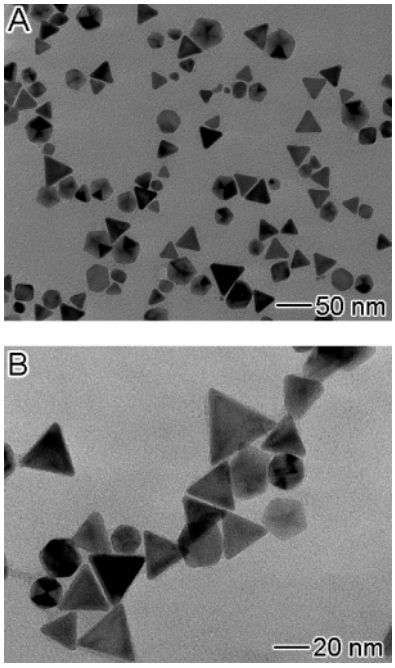

Figure 8. TEM images of a sample prepared under the same conditions as in Figure 1 (at 85 °C in the presence of 0.36 mM $FeCl_3$ and 5 mM HCl, with the molar ratio of PVP to Pd precursor being 5), except the complete exclusion of light from the reaction system.

Effect of Light. As demonstrated in the synthesis of Ag nanoplates, light of appropriate wavelengths was indispensable for the formation of plate morphology.[22,24] To clarify this point, we performed a reaction by completely blocking light from the reaction system. Figure 8 shows typical TEM images of the sample prepared in the absence of light, from which we cannot find distinct morphological difference as compared with the normal synthesis. This result suggests that light is not indispensable for the formation of nanoplates in the case of Pd.

Optical Properties of the Pd Triangular and Hexagonal Nanoplates. The nanoplates are supposed to exhibit SPR features different from those of cubooctahedra or twinned nanoparticles. Figure 9A shows UV−vis extinction spectra taken from aqueous suspensions of the Pd triangular and hexagonal nanoplates; their SPR peaks were located at 520 and 530 nm, respectively. To understand these features, we calculated the spectra using the DDA method. Figure 9B shows the extinction (Q_{ext}), absorption (Q_{abs}), and scattering (Q_{sca}) coefficients (note that $Q_{ext} = Q_{abs} + Q_{sca}$) of a Pd triangular nanoplates of 28 nm in edge length and 5 nm in thickness.[11] The location of the calculated peak matches with the experimentally measured spectrum, albeit the nanoplates seem to display a sharper SPR peak than what is predicted by DDA calculation. Since the polydispersity of as-synthesized samples usually results in broader SPR peaks than those predicted by DDA calculations, the somewhat narrowing of the SPR peaks of Pd nanoplates represents an unusual feature that deserves further investigation. Note that the SPR peaks of Pd nanostructures are all relatively broad, which can be attributed to the dielectric function of Pd.[16]

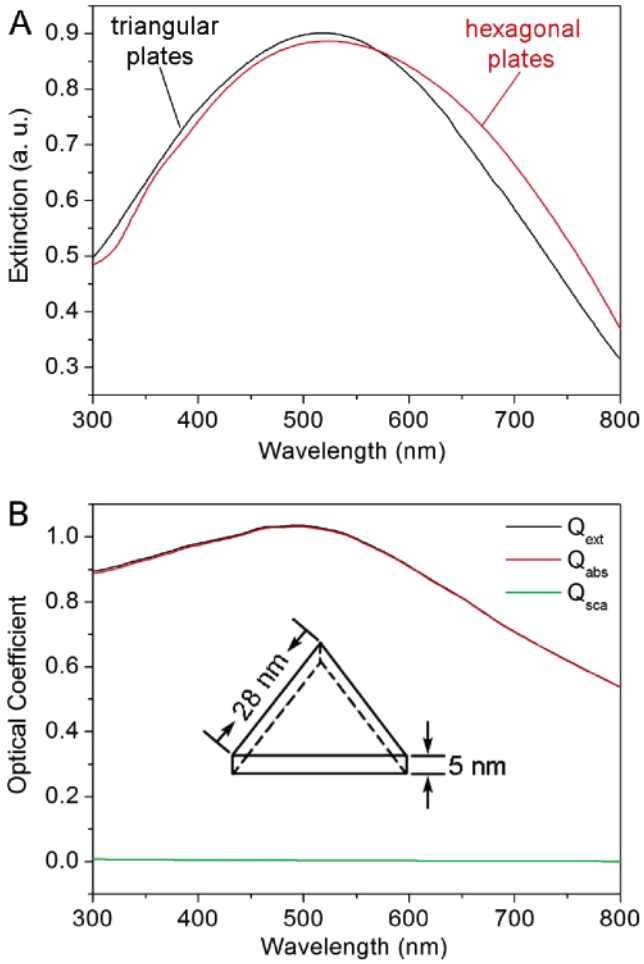

Figure 9. (A) UV−vis extinction spectra of the as-prepared triangular and hexagonal nanoplates shown in Figures 1B and 3C, respectively. (B) The extinction, absorption, and scattering coefficients of a triangular nanoplate as calculated using the DDA method, in which all random configurations of the plate with respect to the incident light were averaged. The optical coefficients were defined as $C/\pi\alpha_{eff}^2$ (with C being cross sections obtained directly from DDA calculation and with α_{eff} being defined through the concept of an effective volume equal to $4\pi\alpha_{eff}^3/3$ for the plate).

Another contribution to the broadening of peaks originates from the thin thicknesses of the plates. As shown in Figure S2, the SPR peak position is dependent on the directions of incident light and electric field polarization relative to the triangular plate. When the field polarization direction is perpendicular to the plate plane, the plate behaves like a regular small spherical particle, whose extinction peak is located in the UV region. In contrast, when the field polarization is parallel to the plate plane, there is a new extinction peak around 520 nm. Considering all random configurations of the plate with respect to the incident light, the SPR peak over the entire spectrum becomes very broad. It is also interesting to note that the scattering coefficient of a Pd triangular nanoplate is negligibly small because the plate is extremely thin. The exceptional wide range of wavelengths across which Pd nanoplates strongly absorb light should make them potentially useful as nanoscale photothermal heating elements.[28]

The Pd nanoplates with well-defined surfaces might serve as ideal substrates for studying the compositional dependence of oxidation, adsorption, and ligand formation on Pd via SERS.[29] As an initial study of the SERS activities of these particles, we have obtained the SERS spectra of 4-mercaptopyridine on Pd triangular and hexagonal nanoplates, in comparison with 8-nm Pd cubooctahedra. As shown in Figure 10, well-resolved SERS spectra could be readily obtained from both Pd triangular and hexagonal nanoplates. In comparison with the spectrum of 8-nm Pd cubooctahedra, the magnitude of signals from triangular and hexagonal nanoplates was 4.3 and 3.4 times stronger. These results indicate that Pd nanoplates are especially active substrates for the SERS detection of molecular species, which is most likely related to the red-shift of SPR peaks, as well as their sharp corners and edges. We expect that these well-defined Pd nanostructures will help to advance the use of Pd in various SERS-related applications.

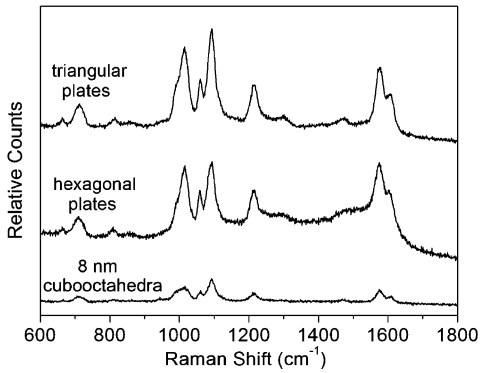

Figure 10. Raman spectra of 4-mercaptopyridine molecules that were adsorbed on Pd triangular nanoplates, hexagonal nanoplates, and 8-nm cuboctahedra.

Conclusion

In summary, we have demonstrated a new strategy for the selective synthesis of Pd triangular and hexagonal nanoplates by manipulating the reduction kinetics of a polyol process. Although rapid reduction of Na_2PdCl_4 by EG in the presence of PVP usually generates thermodynamically favored Pd cubooctahedra and twinned nanoparticles, addition of $FeCl_3$ and HCl could greatly slow the reduction and thus induce the formation of Pd nanoplates. Unlike the previously reported cases of Ag and Au, light was found to play a minor role in the formation of Pd nanoplates.

Since the SPR peaks of Pd nanoparticles less than 10 nm in size are located in the UV region, the SPR properties of Pd nanostructures remain largely unexplored. Here it was demonstrated for the first time that the Pd nanoplates exhibited SPR peaks in the visible region, and their locations were consistent with the results of DDA calculation. Thanks to their sharp corners and edges, the Pd nanoplates were active Pd substrates for SERS detection. It is worth pointing out that the exceptional chemical sensitivity of Pd toward hydrogen should make these Pd nanoplates especially useful for hydrogen storage and SPR-based sensing of hydrogen gas.[14a,30] In addition, these Pd nanoplates might also find use as catalysts, photothermal heating

(28) Hirsch, L. R.; Stafford, R. J.; Bankson, J. A.; Sershen, S. R.; Rivera, B.; Price, R. E.; Hazle, J. D.; Halas, N. J. *Proc. Natl. Acad. Sci. U.S.A.* **2003**, *100*, 13549.
(29) (a) Zou, S.; Weaver, M. J. *J. Phys. Chem.* **1996**, *100*, 4237. (b) Srnová, I.; Vlèková, B.; Baumruk, V. *J. Mol. Struct.* **1997**, *410*, 201. (c) Tian, Z.-Q.; Ren, B.; Wu, D.-Y. *J. Phys. Chem. B* **2002**, *106*, 9463. (d) Gómez, R.; Pérez, J. M.; Solla-Gullón, J.; Montiel, V.; Aldaz, A. *J. Phys. Chem. B* **2004**, *108*, 9943.
(30) Sun, Y.; Tao, Z.; Chen, J.; Herricks, T.; Xia, Y. *J. Am. Chem. Soc.* **2004**, *126*, 5940.

elements, absorption contrast agents, and chemically specific optical sensors.

The present work has clearly established that the introduction of an oxidant into the synthesis of metal nanoparticles can effectively control their nucleation and growth into well-defined sizes and shapes. By combining oxidative etching with the polyol synthesis of Pd nanoparticles, we have achieved selective removal of multiple twinned particles,[20] control of the size of slightly truncated nanocubes,[16a] and deterministic synthesis of triangular and hexagonal nanoplates. Although modification to experimental conditions might be required for different metals, it is expected that the level of shape control that has been realized for Pd should be directly extendible to other metals, as well as the tailoring of properties associated with these metal nanostructures.

Acknowledgment. This work was supported in part by a grant from the NSF (DMR-0451788), a DARPA-DURINT subcontract from Harvard University, and a fellowship from the David and Lucile Packard Foundation. Y.X. is a Camille Dreyfus Teacher Scholar (2002−2007). Y.Y. was supported by the Director, Office of Science, U.S. Department of Energy, under Contract DE-AC03-76SF00098. Z.-Y.L. has been supported by the National Key Basic Research Special Foundation of China (Grant No. 2004CB719804). This work used the Nanotech User Facility (NTUF), a member of the National Nanotechnology Infrastructure Network (NNIN) funded by the NSF. We thank the Molecular Foundry at the Lawrence Berkeley National Laboratory for HRTEM analysis.

Supporting Information Available: Figures showing powder XRD patterns of the as-prepared triangular nanoplates and extinction, absorption, and scattering coefficients of a triangular nanoplate calculated using the DDA method with six different configurations. This material is available free of charge via the Internet at http://pubs.acs.org.

JA056498S